EMERGING OBSTACLES IN SUPERCRITICAL OPEN-CHANNEL FLOWS: DETACHED HYDRAULIC JUMP *VS.* WALL-JET-LIKE BOW-WAVE

N. Riviere[1]
Professor, Université de Lyon, LMFA, INSA de Lyon, 20 av. A. Einstein, 69100 Villeurbanne, France
G. Vouaillat
Graduate Student, Université de Lyon, LMFA, INSA de Lyon, 20 av. A. Einstein, 69100 Villeurbanne, France
G. Launay
Graduate Student, Université de Lyon, LMFA, INSA de Lyon, 20 av. A. Einstein, 69100 Villeurbanne, France
E. Mignot
Associate Professor, Université de Lyon, LMFA, INSA de Lyon, 20 av. A. Einstein, 69100 Villeurbanne, France

Keywords: supercritical flow, open-channel, obstacle, hydraulic jump, wall jet, bridge pier, tsunami

Abstract

A supercritical open-channel flow can skirt an emerged obstacle by using two distinct forms of workaround: a detached hydraulic jump or a so-called "wall-jet-like bow-wave". These two forms stem from the properties of supercritical flow and are described with details. Experiments assess the conditions of appearance of one form or the other, depending on both the upstream Froude number and flow depth to obstacle width ratio. A conceptual model, based on mass conservation, reproduces and explains the corresponding transition. For the wall-jet-like bow-wave, additional information is given regarding the water depth oscillations; the associated Strouhal number show they are caused by the reverse spillage on the obstacle face. Implications of the present results on scouring and on forces exerted by the flow on structures justify future works on the subject.

[1] Corresponding author : nicolas.riviere@insa-lyon.fr

Introduction

Emerging boulders in mountainous watercourses, buildings within the inland flow following a tsunami event, bridge abutments in a flooded floodplain, bridge piers in supercritical rivers in piedmont plains, vehicles in sloping streets during urban floods, avalanche protection devices, *etc.*, are examples of impervious, emerged obstacles embedded in supercritical, open-channel flows. It is observed that the supercritical flow can use two distinct ways of workaround to skirt such obstacles: a detached hydraulic jump or a so-called "wall-jet-like bow-wave". The scientific questions of the present work are the conditions of appearance and the mechanisms associated with each of these two workarounds. First, widely spread results concerning the deflection of a supersonic gas flow are worth reminding, as they present strong analogies with our open-channel supercritical flow problem.

Compressible flows and detached shock waves

An impervious obstacle forces a compressible flow to deviate in order to skirt it. The corresponding workaround adopts different forms, depending on the flow regime and on the obstacle shape. When the flow is subsonic, its velocity is smaller than the speed of sound: disturbances created by the presence of the obstacle can travel upstream. They cause the curvature of the streamlines that ensures the flow deflection. Figuratively speaking, subsonic flows anticipate the presence of the obstacle and the deflection is gradual, through a streamlines curvature. When the flow is supersonic, its velocity is higher than the speed of sound and disturbances created by the presence of the obstacle cannot go back up the flow. Figuratively speaking again, a supersonic flow does not anticipate the presence of the obstacle and the deflection is sudden, through a shock wave that adopts two forms. When the deflection required to skirt the obstacle is small enough (case of slender bodies), an oblique shock wave performs the deflection. The streamlines remain straight lines but experience an

abrupt change of direction through the shock. The limit between such a small deflection and a strong deflection described hereafter (or between a slender and a blunt body) is not purely geometrical. It corresponds to the maximum deflection angle θ_{max} allowed by an oblique shock which depends on the upstream Mach number *M* (Shapiro, 1953) and can be derived using mass and momentum balances (Jaumotte, 1971): θ_{max} is in the range 0-34° for *M*=1-3. If the deflection exceeds this threshold value (case of blunt bodies), a detached shock wave forms upstream from the obstacle. Within the zone delimited by the obstacle and the shock, the flow becomes subsonic and anticipates the presence of the obstacle: the curvature of the streamline is possible and performs the deflection of the flow. Mass and energy considerations allow estimating the detachment length of the shock (Moeckel, 1949) for axisymmetrical bodies, and for 2D obstacles that are more similar to the present problem.

Supercritical open-channel flows and detached hydraulic jumps

Similar phenomena characterize the deflection of an open channel flow by an emerged obstacle. If the flow is subcritical, it deviates progressively through a streamlines curvature, which is additionally combined with backwater effects. If the flow is supercritical, such gradual phenomena are not possible as the flow velocity is higher than the celerity of the gravity waves. In such case, if the deflection is small enough (case of an emerged, sharp obstacle), it is carried out by an oblique hydraulic jump. The maximum deflection angle θ_{max} through such an oblique jump depends on the upstream Froude number *Fr*. From mass and momentum considerations, Ippen (1951) provides a graphical representation of θ_{max} which is in the range 0-33° for *Fr*=1-3. This range is comparable to the one encountered with compressible flows (see preceding section), and was corroborated by experiments on two supercritical flows deflecting each other (Mignot *et al.*, 2008). Considering the analogy with compressible flows, the case of deflection angles exceeding θ_{max} (case of blunt emerged

obstacles) corresponds to the formation of a detached hydraulic jump upstream from the obstacle. Indeed, authors such as Defina and Susin (2006), Mignot and Riviere (2010) or Mignot *et al.* (2016) observed such a detached hydraulic jump around rectangular, wide obstacles. Detached hydraulic jumps also form in supercritical granular flows (Cui and Gray, 2013), as observed in the field around avalanche protection devices (Faug *et al.*, 2015).

The so-called "wall-jet-like bow-wave" and the present scientific issues

However, in the field, the flow observed around blunt obstacles such as bridge piers or boulders in supercritical rivers can take a quite different form, which contradicts apparently the preceding classification of supercritical flow deflections. This form is named herein "wall-jet-like bow-wave", *i.e.* a bow-wave formed by an upward wall-jet on the obstacle upstream face. Photograph of Figure 1 depicts such a flow, around a bride pier, in the "Rivière des Galets", La Réunion Island, France. The flow manages to skirt the obstacle without forming a detached hydraulic jump. Yet, the curvature of the streamlines in the horizontal plane is theoretically impossible as neither a detached hydraulic jump, nor the associated subcritical zone downstream, form. The present paper focuses on this apparent paradox and the competition between the two flow forms: the detached hydraulic jump and the wall-jet-like bow-wave. It is organised as follows. As the work is mainly experimental, section 2 is devoted to describe the two different facilities used. Section 3 provides a detailed description of the two flow forms. Section 4 establishes the conditions of transition from one form to another, which is explained using a conceptual model. Section 5 provides additional characteristics of the wall-jet-like bow-wave: water depth and associated fluctuations in the vicinity of the stagnation point. Section 6 sums-up the main findings of this work, completed by some discussions and prospects.

Physical modelling and experiments

Dimensional analysis

The problem involves parallelepipedal obstacles, within a uniform supercritical flow in a prismatic, rectangular channel. The seven dimensional variables that characterize the flow are thus: the uniform upstream water depth h, the upstream mean velocity U, the obstacle width R, the water properties (density ρ, dynamic viscosity μ and surface tension with air σ) and the gravity acceleration g. Indeed, as the flow is supercritical, the obstacle length (in the streamwise direction) is not considered: it was checked experimentally that it only modifies the wake. Moreover, only parallelepipedal obstacles, emerged with a flat face in front of the flow, are considered herein and R is enough to characterize the whole obstacle shape. Finally, the channel width B is always large enough compared to the obstacle width R so that disturbances induced by the presence of the obstacle reach the walls downstream from the obstacle (see Defina and Susin, 2006), again with no influence on the flow around the obstacle in a supercritical flow. Hereafter, the paper focuses on three flow features which are the flow form (wall-jet-like bow-wave or detached hydraulic jump), the water depth h_{jet} at the stagnation point on the obstacle face and the peak frequency f_p associated with the fluctuations of this water depth. These three features depend on the seven parameters cited above, and this reads:

$$(\text{flow form}, h_{jet}, f_p) = \Phi(h, R, U, \rho, \mu, g, \sigma) \quad (1)$$

Vaschy-Buckingham's Π-theorem, with h as length scale, h/U as time scale and ρh^3 as mass scale, reduces Eq.(1) to a dependency of the three dimensionless flow features on four dimensionless parameters:

$$\left(\text{flow form}, \frac{h_{jet}}{h}, \frac{f_p h}{U}\right) = \Phi\left(\frac{h}{R}, \text{Fr} = \frac{U}{\sqrt{gh}}, \text{Re} = \frac{4\rho U h}{\mu}, \text{We} = \frac{\rho U^2 h}{\sigma}\right) \quad (2)$$

where h/R is the depth to obstacle width ratio, Fr the upstream Froude number, and Re the upstream Reynolds number based on the upstream water depth (justified notably when considering $h<<B$). We is the Weber number that accounts for capillary effects due both to surface tension and local water/air interface curvature. These dimensionless parameters can be rearranged. We can be combined with Fr and Re to form the Morton number Mo (*e.g.* Kobus, 1984 ; Chanson, 2009 ; Mignot and Riviere, 2010) as:

$$\mathrm{Mo} = \frac{g\mu^4}{\rho\sigma^3} = \frac{\mathrm{We}^3}{\mathrm{Fr}^2(\mathrm{Re}/4)^4} \quad (3)$$

Mo depends only on the physical properties of the fluid and on the gravity acceleration. It is constant when considering that both present experiments and typical field engineering situations involve water and air, on earth. Replacing We by Mo suppresses one dimensionless parameter (as Mo is constant): this is beneficial when seeking for an empirical correlation. It should be noted, however, that such a correlation will be invalidated when using other fluids, characterized by another Mo value. Similarly, surface tension effects accounted for by We will not be quantified, as it is addressed in the "Discussion on scale effects" section. Finally, some of the dimensionless parameters are recombined to enhance their physical meaning. It is indeed more meaningful to compare h_{jet} with the kinetic height of the incoming flow (as detailed in section “Properties of the wall-jet-like bow-wave”). In the same way, it is more meaningful to form a Strouhal number St comparing the peak frequency f_p with the time scale $2U/g$ associated with the reverse spillage (as detailed in section “Discussion on scale effects”). Hence, at last, the three flow features of interest depend on the flow characteristics as follows:

$$\left(\text{flow form},\ h_{jet}^{*} = \frac{h_{jet}}{U^2/2g}, S_t = \frac{2f_pU}{g}\right) = \Phi\left(\frac{h}{R}, \mathrm{Fr}, \mathrm{Re}, \mathrm{Mo}\right) = \Phi\left(\frac{h}{R}, \mathrm{Fr}, \mathrm{Re}\right) \quad (4)$$

where Mo is finally discarded as it is a constant. As a brief, all the flow features will depend on three dimensionless parameters: h/R, Fr, Re. Next section describes the experiments used to characterize this dependency.

Experimental Facilities

Two different facilities are used: one water table and one open-channel (Figure 2). Facility 1 is a water table previously used for the study of detached hydraulic jump (Mignot and Riviere, 2010). It is characterized by a very high width to depth ratio B/h allowing thus to avoid any lateral confinement effect (Mignot *et al.*, 2016). The walls are made of glass. The slope can be continuously adjusted up to several percent. The water is provided from a 400L tank through different screens that straighten and smooth the flow. Facility 2 is an open-channel, with adjustable slope, vertical glass walls and a steel bottom (Lelouvetel *et al.*, 2009). Compared to the water table, it is characterized on the one hand by higher discharges and water depths, but on the other hand by a smaller width B=0.25m which imposes experiments with narrow obstacles (namely R<40 mm) to avoid any lateral confinement effect. The water is provided by a constant level tank, fed from an underground sump. Table 1 sums-up the characteristics of these two facilities: width B, useful length L, distance from the entrance to the obstacle L_u, range of discharge Q_v, range of water depth h upstream from the obstacle, range of mean velocities $U=Q_v/Bh$, range of obstacle width R. h is the normal depth, upstream from – and undisturbed by – the obstacle. Indeed, the ratio L_u/h is always higher than 40 in facility 1, higher than 100 in facility 2 so that the flow can be considered as fully developed when reaching the obstacle for most of the experiments. Changing simultaneously the discharge, the channel slope and the obstacle width allows modifying h/R, Fr and Re independently. The corresponding ranges of these dimensionless parameters are given in table 1 for the two facilities.

Instrumentation

In both facilities, an electromagnetic flowmeter measures the discharge and a limnimeter measures the water depth upstream from the obstacle. Associated uncertainties ΔQ_v (discharge) and Δh (upstream water depth) are different for the two facilities and given in table 1. Additionally, water depth elevation and its fluctuations on the obstacle front are measured using conductive wave probes (Wave Monitor, from Churchill Control) with an acquisition frequency of 10 Hz, during 300 seconds. The gap between the two tips is shortened to 2 mm in order to increase the probe sensitivity. The probe is fixed directly on the obstacle upstream face, in the symmetry plane, and its calibration is performed with the same geometry. The uncertainty was estimated to 0.5 mm (Mignot *et al.*, 2008). The signal associated with free-surface oscillations at the stagnation point is then processed to obtain the time-averaged, the standard deviation (not shown here) and the corresponding peak frequencies in the energy spectra provided by FFT with an averaging over short periodograms (Welch, 1967). These experiments are performed only in the open-channel (facility 2) associated to higher velocities; indeed, in the water table (facility 1), the oscillations are of so limited amplitude that no peak frequency can be sorted out from the physical noise created by the free-surface disturbances unavoidable in supercritical flows. Finally, a camera (Manta G-223b, 400Hz at 150x150 pixels, by Allied Vision, associated to an AF Nikkor 20-35mm f/2.8D lens by Nikon) mounted below the transparent bottom and a horizontal laser sheet introduced through the right wall 1mm above the bottom allow to characterize horizontal pathlines in the vicinity of the obstacle by injecting home-made fluorescent particles (as proposed by Pedocchi *et al.*, 2008) with an average diameter 25 μm.

Description of the two flow forms

The detached hydraulic jump in a supercritical, open-channel, water flow was already described by Defina and Susin (2006), Mignot and Riviere (2010) and Mignot *et al.* (2016). In a top view (Figure 3), the jump toe forms a hyperbola, which asymptotes form an angle β_∞ with the upstream flow direction, such as $\sin(\beta_\infty)=1/Fr$. The corresponding detachment length λ_{jump} equals several times the water depth. As the supercritical flow crosses the jump (side view, Fig. 3), it experiences an abrupt water depth increase and experiences locally a subcritical regime. The backwater curve is pronounced, due to the presence of a stagnation point which causes the formation of a small bow-wave, as observed around bridge piers in subcritical rivers (Richardson and Panchang, 1998). This backwater curve causes a strong adverse pressure gradient which promotes the boundary layer separation and the appearance of a horseshoe vortex (Ballio *et al.*, 1998). This vortex strongly interacts with the hydraulic jump both on fixed beds (Mignot and Riviere, 2010; Riviere *et al.*, 2012) and in presence of scouring (Mignot *et al.*, 2016). The pathlines on Figure 4 clearly show that (i) the flow deviates through a streamlines curvature downstream from the toe of the jump and that (ii) the horseshoe vortex detachment length λ_{hsv} is of the order of *h*.

The so-called wall-jet-like bow-wave, described by Figure 5, is significantly different from the detached jump. The flow deviates abruptly upward, very close to the obstacle, at a distance of about one water depth *h* upstream from the obstacle, which is also the scale of the radius of curvature at the jet basis (side view, Figure 5). A vertical wall-jet forms on the upstream face of the obstacle, quite similar to impinging liquid jets in air (*e.g.* Wilson *et al.*, 2012) but with two distinct features. First, the bottom wall forms a 90° angle with the obstacle front face, which acts as a bucket on the flow, causing a deviation from a horizontal to a vertical direction. Second, the lateral confinement exerted by the surrounding, non deflected, supercritical flow prevents the jet from spreading laterally. This is shown by the horizontal

pathlines near the bottom (Figure 6) where, conversely to the detached jump case, no upstream streamline curvature is visible till the very vicinity of the obstacle, *i.e.* a distance of the order of 0.1*h*. The adverse pressure gradient starts at the same location as the jet deflection, so that the streamwise extent of the horseshoe vortex considerably reduces with a detachment length λ_{hsv} of the order of 0.1*h*. As a consequence, the flow is not disturbed by the obstacle until reaching its close surrounding. On the obstacle face, the upward jet separates towards both sides of the stagnation point and forms two lateral jets outing in a top-side diagonal direction from the obstacle corners (top view, Figure 5). The jet, in its upper part, in front of the obstacle, has the form of a breaking bow-wave with a reverse spillage, which causes periodic oscillations of the jet. Indeed, as water from this spillage falls into the supercritical flow, upstream from the obstacle, it suddenly reduces the kinetic energy of the flow, and so the water elevation at the stagnation point. This suppresses the spillage: the upstream flow recovers its initial kinetic energy and this is the beginning of a new cycle. With these wall-jet-like bow-waves, the deflection of the jet is directed in the upward direction. In other words, the discharge blocked by the obstacle is deviated outside from the flow, where it is reintroduced downstream from the obstacle, disregarding of the possible reverse spillage. This is completely different from the hydraulic jump case, where the blocked discharge is deviated laterally and always remains within the main flow.

Condition of appearance of the flow forms

Condition of occurrence of the wall-jet-like bow-wave in experiments

The condition of appearance of one form or the other is correlated to the dimensionless flow parameters by observing the form obtained under a large number of experimental conditions, including both supercritical and subcritical flows. A first set of experiments was performed

239 using the water table facility 1 and a second one using the open-channel facility 2.
240 Corresponding ranges of parameters are listed in table 1. These two sets are plotted on Figure
241 7, in a (Fr, *h/R*) plane. The open symbols correspond to the upward deflection of the flow by a
242 wall-jet-like bow-wave and are all located in the upper part of the graph and for Fr>1. The
243 closed symbols correspond to a crosswise deflection of the flow by a streamline curvature and
244 backwater effects downstream a hydraulic jump (case of a supercritical upstream flows, Fr>1)
245 or throughout the whole flow (case of a subcritical regime, Fr<1).

246 Among the three parameters provided by Eq.(4), the couple of parameters (Fr, *h/R*) is clearly
247 a selective criterion to characterize the flow typology. It is not the case for the Reynolds
248 number, as shown by the overlap of the two datasets obtained in the two facilities (triangles
249 for facility 1, squares for facility 2) with quite different ranges of Re (see table 1). In the
250 subcritical regime, no wall-jet-like bow-wave exists as the flow deflection starts upstream
251 from the obstacle: this is illustrated on Figure 7 by the sudden transition at Fr=1 from a wall-
252 jet-like bow-wave to a crosswise deflection, for h/R>2. Now, in the supercritical regime, for a
253 given Froude number, the wall-jet-like bow-wave occurs for high h/R ratios and the detached
254 jump for smaller ones. For a given h/R ratio, the wall-jet-like bow-wave occurs for high
255 Froude numbers. As a brief, the increase of both h/R and Fr favours the appearance of the
256 wall-jet-like bow-wave. The conceptual model developed in next sections explains this
257 behaviour.

258 *Conceptual model explaining the transition*

259 The deflection of the flow, either upward (wall jet) or crosswise (jump) is ruled by the mass
260 conservation: the impervious obstacle blocks a part Q_{in} of the incoming flow, which must be
261 evacuated elsewhere. As the flow is supercritical, Q_{in} simply reads:

262 $$Q_{in} = RUh \tag{5}$$

Considering a wall-jet-like bow-wave, the discharge evacuated by the jet is estimated considering Figure 5. Assuming energy conservation from the flow to the jet initial horizontal section, the kinetic energy is also conserved as the sum of potential energy and pressure is constant. The velocity at the jet base is thus U. Considering mass conservation, with a velocity U, the jet section is still ($R.h$). As its width is R, its thickness (in the streamwise direction) is h. This thickness decreases as and when the jet goes up, due to mass losses caused by lateral evacuation, and its average value is $e=C_1.h/2$. The jet can reach, at the stagnation point, a maximum height $h_{jet\text{-}max}=(C_2.C_3)U^2/2g$ above the upstream flow, where C_2 and C_3 are constants that account respectively for head-losses ($C_2<1$) and for the kinetic energy coefficient upstream in the flow ($C_3>1$). The mean transverse outlet velocity is noted u_{out}, assumed such as $u_{out} = C_4U$ where C_4 ($C_4<1$) is a constant that accounts for both head losses and kinetic to potential energy transfers in the wall-jet. By considering $C=C_1C_2C_3C_4$, the maximum discharge $Q_{out\text{-}max}$ that can be evacuated through the two-sides of the wall-jet reads:

$$Q_{out-\max} = 2e\, h_{jet-\max}\, u_{out} = CU\frac{U^2}{2g}h \qquad (6)$$

The wall-jet-like bow-wave exists if and only if the jet is able to evacuate all the discharge blocked by the obstacle, in other words if $Q_{out\text{-}max} \geq Q_{in}$. Considering eqs. (5&6), this leads to:

$$\frac{h}{R} > \frac{2}{C \cdot \mathrm{Fr}^2} \qquad (7)$$

This limit is plotted on Fig. 7, using C=1.1, and restricted, of course, to Fr>1. It corresponds fairly well to the transition observed experimentally. Most of the points corresponding to a wall-jet-like bow-wave are located above this limit, while most of those corresponding to a detached-hydraulic jump are located below. Hence, the mechanism, leading to one form or another, appears to be well understood, it simply relies on the mass conservation. For high h/R

ratios, corresponding to thin blunt (parallelepipedal) obstacles, the wall-jet is able to evacuate the flow blocked by the obstacle. For small h/R ratios, corresponding to obstacles that are wide with regards to the water depth, the wall-jet is not able to evacuate the whole blocked discharge ($Q_{out\text{-}max} < Q_{in}$). Water must skirt the obstacle laterally, within the flow, and this requires a streamlines curvature. The latter can be obtained only within a subcritical regime. Thus, a hydraulic jump forms and replaces the wall-jet.

Transition and asymptotic behaviours

Devoted experiments are undergone to characterize the transition from one form to another, across the limit plotted in Figure 7. To do so, for a few given slopes, the discharge is decreased little by little to pass from a wall-jet-like bow-wave to a jump and then increased little by little to recover a wall-jet. These experiments show no hysteresis effect: the transition occurs for the same discharge, *i.e.* for the same (Fr, h/R) value in both cases. More, these experiments reveal that the transition is not a brutal phenomenon: starting from a wall-jet-like bow-wave, when decreasing little by little h/R and in a lesser extent Fr (by decreasing little by little the discharge for a fixed slope), the reverse spillage is at first very rare, and then occurs more often, creating each time, temporarily, a subcritical zone (and thus a detached jump) upstream from the obstacle. When the reverse spillage occurs most of the time, the subcritical zone remains almost all the time and this leads to the occurrence of the permanent detached hydraulic jump. This indicates that the limit between the two forms in the (Fr, h/R) plane (Figure 7) is somehow subjective. To obtain the points of Figure 7, the following strategy is used in the channel (facility 2): for a fixed h/R value, starting with a detached jump, the Froude number is increased until an oscillation of the water depth on the obstacle front face is observable. This indicates a spillage and is considered as the transition to the wall-jet-like bow-wave. In the water table (facility 1), this transition is obtained as follows: the discharge is

increased little by little for a given slope, thus increasing h/R and increasing Fr at the same time.

Note moreover that for high h/R values, the wall-jet-like bow-wave becomes similar to the bow-wave around a ship-stem (*e.g.* Delhommeau *et al.*, 2009). In this case, the blocked discharge Q_{in} is rapidly evacuated by the jet: the height on the obstacle face is clearly smaller than the kinetic height, *i.e.* $h_{jet}<h_{jet\text{-}max}$, and the thickness e of the jet rapidly decreases and becomes significantly smaller than h.

Properties of the wall-jet-like bow-wave

The detached hydraulic jump configuration was deeply investigated by Mignot and Riviere (2010) and the present section is devoted to describe the other flow form considered herein: the wall-jet-like bow-wave. With this flow form, the stagnation point is associated to water depth elevation and oscillations.

Time-averaged water depth at the stagnation point

The time-averaged jet height above the flow is h_{jet} (Figure 5). Its measured values, once made dimensionless relative to the kinetic height, so that $h_{jet}^{*}= h_{jet}/(U^2/2g)$, are sketched on Figure 8-a, as a function of the Froude number, for different values of the depth to obstacle width ratio h/R. The closed symbols correspond to hydraulic jumps. Watching the open symbols, corresponding to wall-jet-like bow-waves, h_{jet}^{*} decreases as both Fr or h/R increase. This can be explained again by the mass conservation. Indeed, with $Q_{out\text{-}max} > Q_{in}$, all the discharge Q_{in} is evacuated before the wall-jet reaches the kinetic height and $h_{jet}<h_{jet\text{-}max}$. In other words, $h_{jet}/h_{jet\text{-}max}$ decreases if $Q_{in}/Q_{out\text{-}max}$ decreases. Yet, from Eq. (7), the ratio $Q_{in}/Q_{out\text{-}max}$ reads:

$$\frac{Q_{in}}{Q_{out-\max}} = \frac{2/C}{\mathrm{Fr}^2 \frac{h}{R}} \quad (8)$$

This confirms that both $h_{jet}/h_{jet\text{-}max}$ and $h_{jet}^* = C_2.C_3.(h_{jet}/h_{jet\text{-}max})$, following the behaviour of $Q_{in}/Q_{out\text{-}max}$, decrease when increasing h/R (due to a decrease of Q_{in}) or when increasing Fr (due to an increase of both $h_{jet\text{-}max}$ and $Q_{out\text{-}max}$). Incidentally, h_{jet}^* is correctly fitted by the following correlation:

$$h_{jet}^* = 1.7\left(\frac{h}{R}\right)^{-0.24} Fr^{\left(-0.24\frac{h}{R}-0.17\right)} \quad (9)$$

which coefficients were determined using a least squares method. The agreement is shown by Figure 8-b, where the correlation provides results in the (-5%; +10%) range from experimental ones. Finally, it is worth noting that values $h_{jet}^*>1$ are encountered. This is possible considering that the surface velocity U_{surf} is higher than the mean velocity U. A classical estimate of this velocity is $U_{surf} = U/0.8$ (*e.g.* Graf and Altinakar, 2000) and corresponds indeed to an upper bound of $h_{jet}/(U^2/2g)$ which is $1.6 \approx (1/0.8)^2$, depicted by the dashed line in Figure 8-a.

Water depth fluctuations

In case of a wall-jet-like bow-wave, the water depth fluctuations at the stagnation point exhibit a clear peak frequency f_p that increases when Fr (Figure 9-a) or h/R (not shown here) increases. A Strouhal number St is defined to check the dependency of these depth fluctuations on the flow parameters and reads:

$$St = \frac{2U}{g} f_p \quad (10)$$

This number is the ratio of a characteristic time of advection in the flow, $2U/g$, and of the characteristic time of the water depth fluctuations, namely $1/f_p$. $2U/g$ is twice U/g which is a

characteristic time both for water to climb up to the stagnation point located at a height $U^2/2g$ above the free-surface, and for water to fall from this stagnation point down to the free-surface (free-fall under gravity in the spillage). The St values are sketched on Figure 9-b: they are distributed around an average value St=0.84, for all the experiments with $R \geq 20$mm. This fixed value indicates that the time scale $2U/g$ is relevant and that the oscillating phenomenon is linked to climbing and then falling down water associated with the reverse spillage. However, Strouhal numbers differ for very small obstacle widths R (R=10mm in Fig. 9-b), while no oscillations are observed for very small water depths h, and this is discussed in the next section, devoted to scale effects

Discussion on scale effects

The wall-jet-like bow-waves produced in the laboratory appear to be very similar to the ones occurring in the field and depicted by Figure 1. However, as h or R strongly reduces, scale effects occur as capillary effects become noticeable.

Obtaining small h/R values (namely $h/R<0.5$) requires – at least with the present experimental facilities – producing flows with small water depths. In this case, the jet presents an alternative form named here "clinging bow-wave". The water depth is almost constant at the stagnation point, forms an upper roll edge with no reverse spillage and with the jet clinging on the lateral walls of the obstacle. To check if this phenomenon is due to pressure effects, as it is for a clinging nappe on a sharp crest weir, a rectangular plate replaces the obstacle. This plate is an obstacle with negligible longitudinal length, and thus with no lateral walls, but same width R as the obstacle. The jet on the plate face is not modified compared to the one obtained with the standard obstacle. This shows that pressure effects on the lateral walls are not responsible for the formation of the clinging bow-wave. The latter is rather attributed to

capillary effects. Dimensional analysis in Eq.4 showed that all flow physical phenomena are accounted for by the quartet (h/R, Fr, Re, Mo). It is nevertheless useful to go back to the Weber number as in Eq.2, as We gives relevant indications on the importance of these capillary effects. Yet, a relevant length scale to compute this number is available: it is the minimum radius of curvature at the air/water interface. We thus reads:

$$\mathrm{We} = \frac{\rho U^2}{\sigma} \min(h, R) \tag{11}$$

Clinging bow-waves correspond actually to the smallest values of the Weber number of the present experimental dataset (table 1), and present the same features as surface tension driven wall jets, notably the upper roll edge referred as "film jump" by Wang *et al.* (2013). Unfortunately, models from these authors cannot be used herein as the present jet (i) with bigger scales, remains mainly driven by gravity rather than by capillary effects, and (ii) does not have a round section.

Oppositely, flows with high h/R values (higher than 3) are produced in the channel using small width obstacles (R=10mm) to avoid any lateral confinement effect. With such narrow obstacles, some-millimetres long elongated drops form at the jet tip and this is attributed to capillary effects. This jet modification does not infer with the time averaged water depth on the obstacle frontal face (plotted on Figure 8). Conversely, the new jet form modifies the unsteady behaviour of the wall jet. A second frequency peak appears in the energy spectra associated with the water depth variations, which is not a harmonic of the first one. It is attributed to the free-fall of the elongated drops. The corresponding Strouhal numbers are included on Figure 9-b (open symbols, with two St values for each (Fr, h/R) value) where they form two populations: smaller values of about St≈0.6 and higher values of about St≈1.7. This is different from the single average values of about St≈0.84 obtained for the wider obstacles, (R>20mm).

Such capillary effects are negligible at the field-scale relevant to hydraulic engineers. At the laboratory scale, they do not influence the transition from a wall jet to a hydraulic jump. They can modify the wall jet features and this may be experienced in other small-scale experiments.

Concluding remarks and discussion

This paper dealt with the two flow forms that can be encountered around a rectangular, emerged obstacle embedded in a supercritical, open-channel flow. A first one is the "detached hydraulic jump", for which the workaround of the obstacle is promoted by a streamlines curvature, in a horizontal plane, allowed by the subcritical region between the jump and the obstacle. A second one is the so-called “wall-jet-like bow-wave”, for which the flow remains supercritical until it reaches the obstacle, preventing from any streamline curvature in the horizontal plane to skirt the obstacle. This apparent paradox – with a reasoning based on the knowledge on 2D compressible flows – is explained by one property of the open-channel flow: its vertical confinement between the bottom and the free-surface. Through the wall-jet, the water can leave this confined region between the bed and the free-surface and the workaround is performed outside from the main flow, without requiring a horizontal streamline curvature. However, such a jet is not always able to evacuate all the water blocked by the obstacle, especially when the obstacle width R becomes noticeably higher than the water depth h. In this case, a detached hydraulic jump forms and replaces the wall-jet-like bow-wave. The threshold ratio h/R, corresponding to this transition, decreases with the Froude number, in agreement with a conceptual model that shows that the transition is driven by mass conservation. Focusing on the wall-jet-like bow-wave, the wall-jet height above the flow is also driven by mass conservation. It depends both on Fr and h/R, as summed-up by an empirical correlation. Finally, the wall-jet is subject to height oscillations: the associated

Strouhal number was found to be constant, confirming that these oscillations correspond to a cycle of climbing-falling down water associated to the reverse spillage on the upstream face.

Discussion

Nevertheless, still considering emerged obstacles, the present results may be quantitatively modified by changing the obstacle shape. In presence of a wall-jet-like bow-wave, more streamlined obstacles – such as obstacles with circular or ovoid horizontal sections that are more representative of bridge piers – may facilitate the flow evacuation by the side jets. The two flow forms will exist but the threshold curve $h/R=f(\mathrm{Fr})$ marking the transition from one to the other is expected to be lowered: the wall-jet-like bow-wave should form for smaller h/R for a given Fr. The present results will also be modified when considering weakly emerged obstacles. Part of the wall jet discharge will be evacuated above the obstacle, facilitating the appearance of a wall-jet-like bow-wave *i.e.* again shifting the transition to smaller h/R values. This corresponds typically to almost emerging boulders in supercritical rivers.

Present results may be used in different hydraulic engineer's applications. A first one is risk mitigation. The supercritical flow encountered in sloppy streets during urban floods (Mignot *et al.*, 2006) or within the inland flow following immediately a tsunami event (Matsutomi *et al.*, 2001 ; Nandasena *et al.*, 2012) will interact differently with different kind of obstacles. For a given Froude number, a wall-jet-like bow-wave will form around bridge piers with $h/R>1$, as corroborated by the observations of Motley *et al.* (2015) but conversely, a detached hydraulic jump will form around a building with $h/R<1$, as corroborated by Testa *et al.* (2007) where the jumps formed around different buildings interact, causing a global increase of the water depth in a model city. More generally, the results foreshadow huge variations of the force exerted by supercritical flows on obstacles (building, piers, vehicles …) as the water depth elevation h_{jet} on the obstacle face can be significantly smaller than the kinetic height

$U^2/2g$. For the hydraulic jump, this is due to energy dissipation which depends on the Froude number. For the wall-jet-like bow-wave, it was shown that $h_{jet}/(U^2/2g)$ depends both on Fr and h/R. Future work should be devoted to characterize these forces. A second hydraulic engineer's application related to the present results is scouring in supercritical flows. Boyer and Roy (1991) show that, in supercritical regime, the scour depth upstream a boulder-like obstacle is proportional to the water depth in front of the obstacle. This is consistent with Mignot *et al.* (2016) who, in presence of a detached hydraulic jump, observed no fundamental changes in the inception of scouring compared to subcritical flow cases. Indeed, upstream from the obstacle, the flow reaches a subcritical regime through the jump; skirting the obstacle, it accelerates at the upstream corners, increasing there the bed shear and causing the scour inception, as observed in fully subcritical flow regimes (*e.g.* Diab *et al.*, 2010). In presence of a wall-jet-like bow-wave, the lateral jets evacuate the discharge "outside" from the flow and suppress the acceleration at the obstacle corners. Moreover, the water depth at the obstacle stagnation point differs with a hydraulic jump and a wall-jet, and depends on the two dimensionless parameters (Fr, Re). Hence, by modifying both velocities and water depth, wall-jet-like bow-waves are expected to influence the scouring at the toe of piers, and this should be addressed in future works.

Acknowledgements

Authors thank S. Roux (CNR, Lyon, France) and F. Fruchart (Easy Hydro, France) for fruitful discussions about the field case of "La Rivière des Galets", Ile de la Réunion, France. Authors are indebted to the "Direction de l'Environnement, de l'Aménagement et du Logement de la Réunion (DEAL 974)," concerning the photograph of Figure 1.

References

Ballio, F., Bettoni, C., and Franzetti, S. (1998). A survey of time-averaged characteristics of laminar and turbulent horseshoe vortices. *Journal of Fluids Engineering*, 120(2), 233-242.

Boyer, C., and Roy, A. G. (1991). Morphologie du lit autour d'un obstacle soumis à un écoulement en couche mince. *Géographie Physique et Quaternaire*, 45(1), 91-99 (in French).

Chanson, H. (2009). Turbulent Air-water Flows in Hydraulic Structures: Dynamic Similarity and Scale Effects. *Environmental Fluid Mechanics*, 9(2), 125-142.

Cui, X., and Gray, J. M. N. T. (2013). Gravity-driven granular free-surface flow around a circular cylinder. *Journal of Fluid Mechanics*, 720, 314-337.

Defina A. and Susin F. M. (2006). Multiple states in open channel flow, in vorticity and turbulence effects in fluid structures interactions. *Advances in Fluid Mechanics*, edited by M. Brocchini and F. Trivellato, WIT Press, Southampton, UK, 2006 pp. 105–130.

Delhommeau, G., Guilbaud, M., David, L., Yang, C., and Noblesse, F. (2009). Boundary between unsteady and overturning ship bow wave regimes. *Journal of Fluid Mechanics*, 620, 167-175.

Diab, R., Link, O., and Zanke, U. (2010). Geometry of developing and equilibrium scour holes at bridge piers in gravel. *Canadian Journal of Civil Engineering*, 37(4), 544-552.

Faug T., Childs P., Wyburn E., Einav I. (2015). Standing jumps in shallow granular flows down smooth inclines, *Physics of Fluids*, 27, 073304.

Graf, W. H., and Altinakar, M. S. (2000). Hydraulique Fluviale, Traité de Génie Civil, vol. 16. *Presses Polytechniques et Universitaires Romandes*.

Ippen, A. T. (1951). "Mechanics of supercritical flow: 1st paper of high velocity flow in open channels: A symposium." *Transactions of the ASCE*, 116, 268–295.

496 Jaumotte, A. L. (1971). *Chocs et ondes de choc*. Paris: Masson.
497 Kobus, H. (1984). Local Air Entrainment and Detrainment. *Proc. Intl Symp. on Scale Effects*
498 *in Modelling Hydraulic Structures* (*IAHR),* Esslingen, Germany, H. Kobus Editor, Paper
499 4.10.
500 Lelouvetel, J., Bigillon, F., Doppler, D., Vinkovic, I., and Champagne, J. Y. (2009).
501 Experimental investigation of ejections and sweeps involved in particle suspension. *Water*
502 *Resources Research*, 45(2).
503 Matsutomi, H., Shuto, N., Imamura, F., and Takahashi, T. (2001). Field survey of the 1996
504 Irian Jaya earthquake tsunami in Biak Island. *Natural Hazards*, 24(3), 199-212.
505 Mignot, E., Paquier, A., and Haider, S. (2006). Modeling floods in a dense urban area using
506 2D shallow water equations. *Journal of Hydrology*, 327 (1–2), 186–199.
507 Mignot, E., Riviere, N., Perkins, R. and Paquier, A. (2008). Flow patterns in a four-branch
508 junction with supercritical flow. *Journal of Hydraulic Engineering*, 134(6), 701-713.
509 Mignot, E. and Riviere, N. (2010). Bow-wave-like hydraulic jump and horseshoe vortex
510 around an obstacle in a supercritical open channel flow. *Physics of Fluids*, 22(11), 117105.
511 Mignot, E., Moyne, T., Doppler, D., Riviere, N. (2016). Clear-Water Scouring Process in a
512 Flow in Supercritical Regime. *Journal of Hydraulic Engineering*, 142(4), 04015063.
513 Moeckel, W. E. (1949). Approximate method for predicting form and location of detached
514 shock waves ahead of plane or axially symmetric bodies. *In NACA TN D-1921*.
515 Motley, M. R., Wong, H. K., Qin, X., Winter, A. O., Eberhard, M. O. (2015). Tsunami-
516 induced forces on skewed bridges. *Journal of Waterway, Port, Coastal, and Ocean*
517 *Engineering*, 142(3), 04015025.
518 Nandasena, N. A. K., Sasaki, Y., and Tanaka, N. (2012). Modeling field observations of the
519 2011 Great East Japan tsunami: Efficacy of artificial and natural structures on tsunami
520 mitigation. *Coastal Engineering*, 67, 1-13.

Pedocchi F., Martin J.E., García M.H. (2008). Inexpensive fluorescent particles for large-scale experiments using particle image velocimetry. *Experiments in Fluids*, 45(1), 183‑186.

Richardson, J. and Panchang, V. (1998). Three-Dimensional Simulation of Scour-Inducing Flow at Bridge Piers. *Journal of Hydraulic Engineering*, 124(5), 530–540.

Riviere N., Laïly G., Mignot E., Doppler D. (2012). Supercritical flow around and beneath a fixed obstacle. *2nd IAHR Europe Congress*, June 27-29 2012, Munchen, Germany.

Shapiro, A. H. (1953). *The dynamics and thermodynamics of compressible fluid flow.* New York: Ronald Press, 1953-54, 1.

Testa, G., Zuccala, D., Alcrudo, F., Mulet, J., and Soares-Frazão, S. (2007). Flash flood flow experiment in a simplified urban district. *Journal of Hydraulic Research*, 45, 37-44.

Wang, T., Davidson, J. F., and Wilson, D. I. (2013). Effect of surfactant on flow patterns and draining films created by a static horizontal liquid jet impinging on a vertical surface at low flow rates. *Chemical Engineering Science*, 88, 79-94.

Welch, P. D. (1967). The use of fast Fourier transform for the estimation of power spectra: A method based on time averaging over short, modified periodograms. *IEEE Transactions on Audio and Electroacoustics*, 15(2), 70-73.

Wilson, D. I., Le, B. L., Dao, H. D. A., Lai, K. Y., Morison, K. R., and Davidson, J. F. (2012). Surface flow and drainage films created by horizontal impinging liquid jets. *Chemical Engineering Science*, 68(1), 449-460.

541

542 Table 1. Characteristics of the two experimental facilities

	Facility 1 (water table)	Facility 2 (channel)
Width B (m)	0.75	0.25
Length L (m)	1.2	9.24
L_u (m)	0.5	5
Q_v (L/s)	0.25 - 3.2	0.51 - 21.89
ΔQ_v	± 0.05 L/s	± 1 %
h (mm)	1.28 - 12.33	10 - 50
Δh (mm)	± 0.25	± 0.5
R (mm)	13 - 100	10 - 50
L_u/h	40.6 - 391	100 - 500
h/R	0.012 - 2.57	0.3 - 4
Fr	0.56 - 6.35	0.5 - 2.7
Re	1300 - 16000	10000 - 208000
We	1 - 50	5 - 800

543

544

Figure 1. Photograph of the wall-jet-like bow-wave around a bridge pier in the "Rivière des Galets", La Réunion Island, France, in March 2006. Courtesy of Paul Bonnet, DEAL 974 (ex DDE 974)

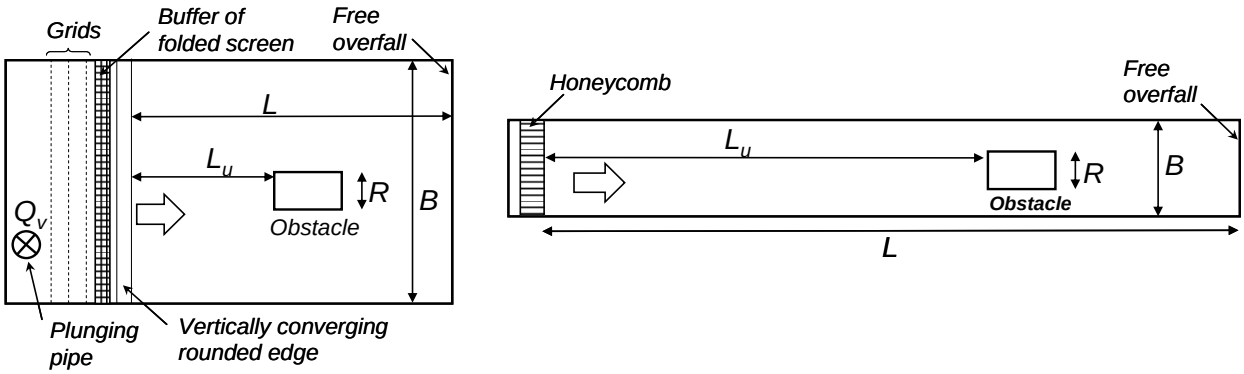

Figure 2. Schematic, top views of facilities 1(left) and 2(right)

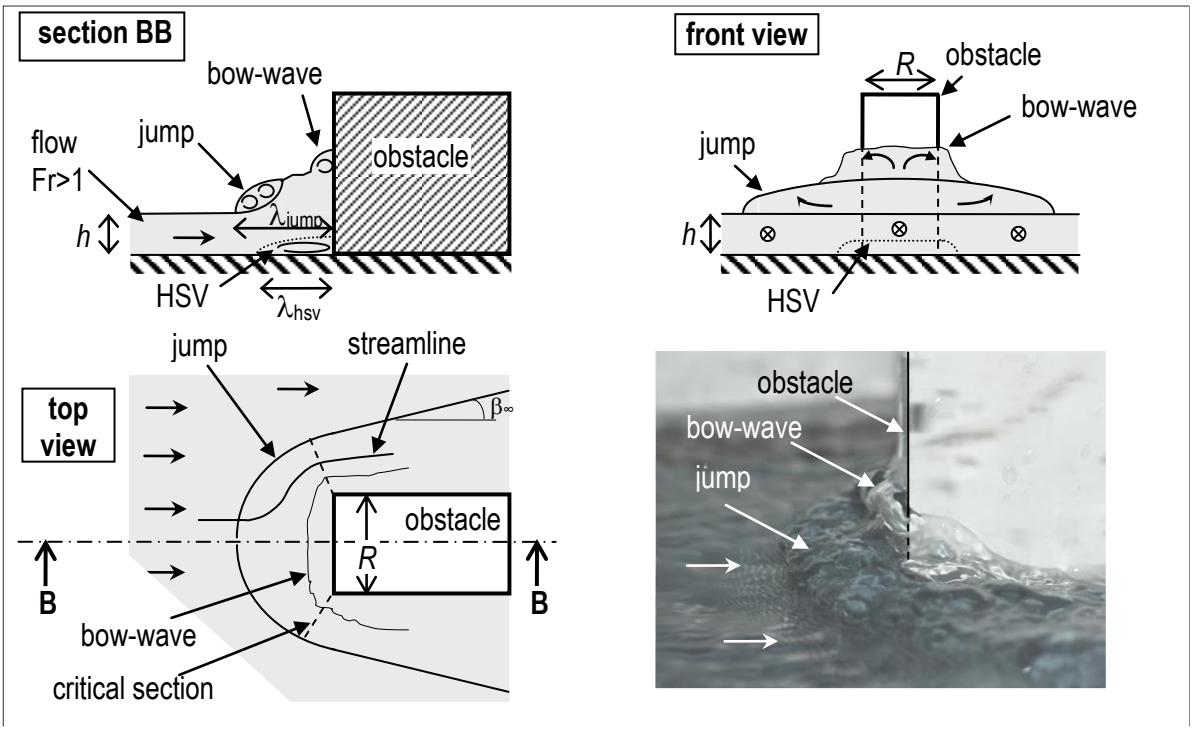

Figure 3. Detached hydraulic jump around a rectangular obstacle: schematics and photograph.

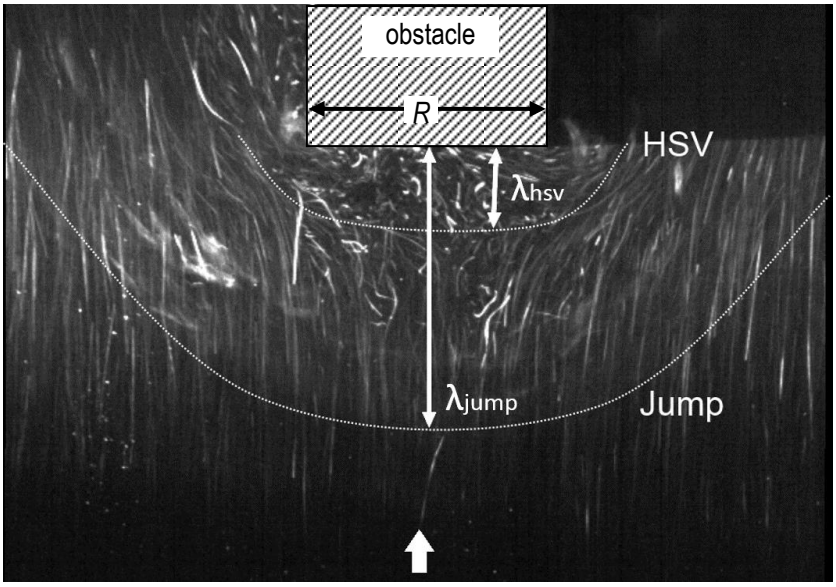

Figure 4. Pathlines below a detached hydraulic jump using a time-exposure photograph (Facility 1; R = 20 mm; U = 0.652 m/s; h = 5.14 mm ; $\lambda_{jump} \approx 20$ mm and $\lambda_{hsv} \approx 6$ mm). Note that the top-right region of the photograph is dark due to the obstacle shadow.

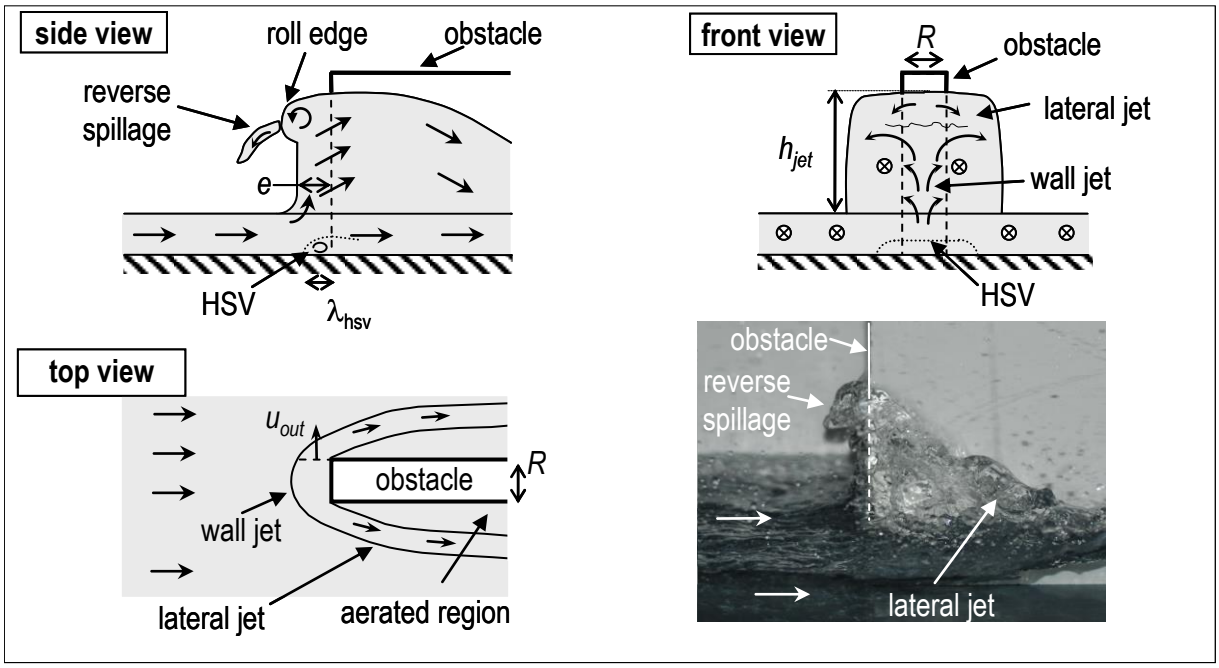

Figure 5. Wall-jet-like bow-wave around a rectangular obstacle: schematics and photograph

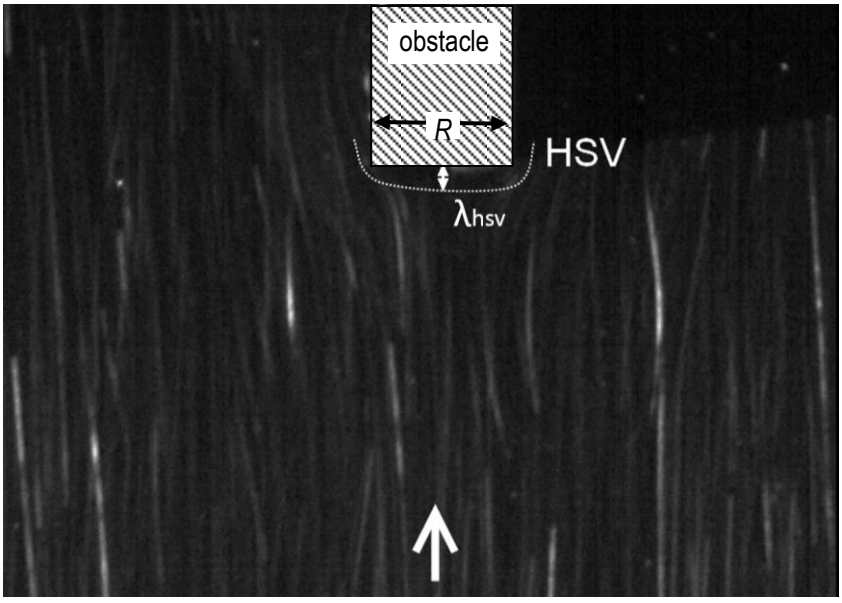

Figure 6. Pathlines below a wall-jet-like bow-wave using a time-exposure photograph (Facility 1; R = 6 mm; U = 0.652 m/s; h = 5.14 mm; $\lambda_{hsv} \approx 0.8$ mm.)

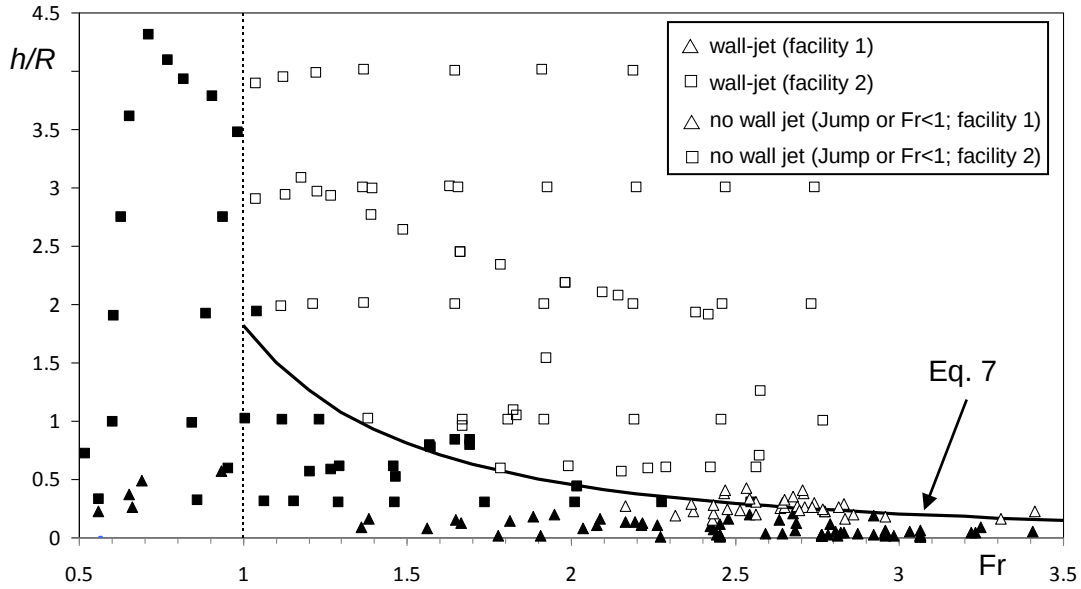

Figure 7. Flow forms plotted in the (Fr, h/R) plane, reported from present experiments.

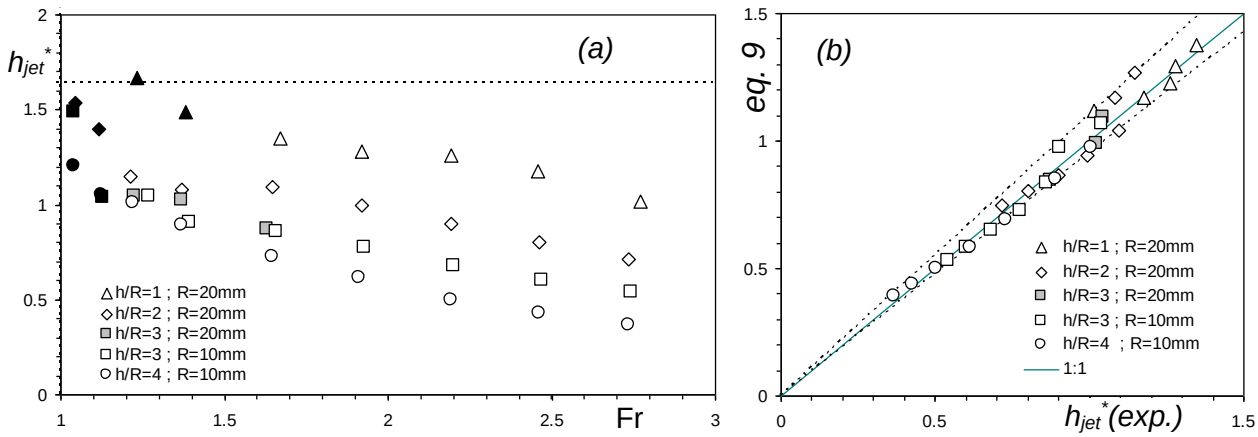

Figure 8. (a) Time-averaged relative jet height $h_{jet}^{*} = h_{jet}/(U^2/2g)$ measured in the channel (facility 2) as a function of the upstream Froude number, for different h/R values; open symbols correspond to a wall-jet-like bow-wave while closed symbols correspond to a hydraulic jump. (b) Comparison of the empirical correlation (Eq. 9) with the experimental data.

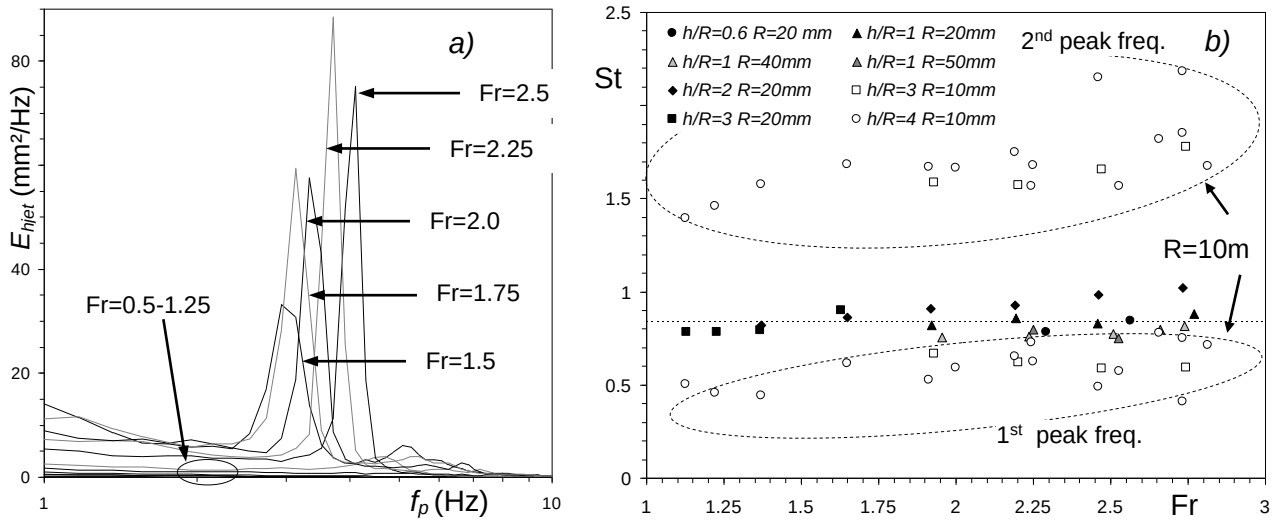

Figure 9. a) Example of frequency spectra associated with water depth fluctuations on the obstacle upstream face for h/R=2 and increasing Froude numbers, obtained in facility 2 and b) Strouhal numbers corresponding to water depth fluctuations on the obstacle upstream face as a function of the upstream Froude number, for different h/R values.